Surface Charge and Field Distribution in a Finite SAW Transducer

VELIMIR M. RISTIC, MEMBER, IEEE, AND ALI M. HUSSEIN, STUDENT MEMBER, IEEE

Abstract—**Using the moment-method technique, closed-form expressions for the surface charge, potential and electric fields of a finite transducer over a low coupling substrate are derived. The influence of the end effects on the total capacitance of the transducer are studied and the field patterns of three different electrode sequences are computed. It is shown that for Y–Z lithium niobate, the surface-charge density is proportional to the normal component of the electric field under the transducer. The moment-method technique was also used to study the total input admittance of finite transducers on Y–Z lithium niobate as a function of the number of finger pairs. Numerical results indicate that the increase in capacitance and conductance with the number of finger pairs, when the number of finger pairs exceeds three, is approximately constant.**

I. Introduction

In STUDIES and applications of SAW devices the determination of the quasi-static charge distribution on interdigital transducers is of interest [1]–[5]. Most of the previous treatments of this problem assumed an infinitely long transducer geometry in order to avoid the consideration of the end effects [1]–[3], [6]–[8]. This assumption is well justified for long transducers of constant or low varying periodicity. Certain aspects of the problem, in finite geometry, were treated by Hartmann and Secrest [9] who used an iterative technique to find the field distribution at the end of the transducer. More recently, Smith and Pedler [4] reduced the problem of a finite transducer to a set of linear equations, and obtained expressions for the charge density and electric field at the surface of the substrate, useful in the equivalent circuit modeling.

In this paper a moment method [10], [11] is used to find the surface-charge density of a finite transducer. A closed-form expression for the electric field at any point under the transducer is obtained. Furthermore, no numerical integration is necessary in the calculation of the surface charge, capacitance, and field distribution. The expressions derived can be used as the forcing term in the inhomogeneous elastic problem [1], and the technique can be easily extended to include transducers with layered structures [7], [8] as well as for determination of the exact charge distribution in transducers on high-piezoelectric coupling substrates [12].

Manuscript received June 23, 1978; revised December 4, 1978. This work was supported by the National Research Council of Canada.

V. M. Ristic is with the Department of Electrical Engineering, University of Toronto, Toronto, Ont., Canada M5S 1A4.

A. M. Hussein was with the Department of Electrical Engineering, University of Toronto, Toronto, Ont., Canada. He is now with the National Research Council of Canada, Ottawa, Canada.

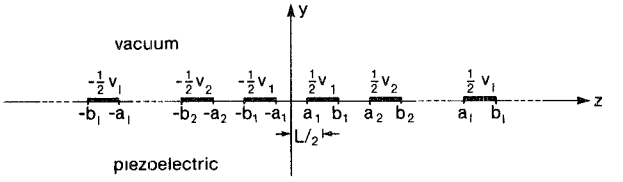

Fig. 1. The geometry of the transducer of finite length.

The analysis is carried out in the limit of the zero-piezoelectric coupling in the geometry shown in Fig. 1. In both, vacuum and piezoelectric $\nabla\cdot\vec{D}=0$, and in the piezoelectric $\vec{D}=-\overleftrightarrow{\epsilon}\cdot\nabla V$, where $\vec{D}$, $\overleftrightarrow{\epsilon}$, and V are the displacement, permittivity tensor, and potential, respectively. The metallic strips, in the transducer, are assumed long enough so that the transverse effects can be neglected. In the piezoelectric medium, $\nabla\cdot\vec{D}=0$ reduces to [9]

$$\epsilon_{22}\frac{\partial^2 V}{\partial y^2}+2\epsilon_{23}\frac{\partial^2 V}{\partial y\partial z}+\epsilon_{33}\frac{\partial^2 V}{\partial z^2}=0. \tag{1}$$

The potential in the vacuum ($y>0$) and in the piezoelectric ($y<0$) can be expressed as

$$V(y,z)=\frac{1}{2\pi}\int_{-\infty}^{+\infty}A(k)\exp\left[\psi(k,y)y-jkz\right]dk \tag{2}$$

where

$$\psi(k,y)=\begin{cases}jk\epsilon_{23}/\epsilon_{22}+\epsilon_r|k|, & y<0\\ -|k|, & y>0\end{cases} \tag{3}$$

and

$$\epsilon_r=\left(\epsilon_{22}\epsilon_{33}-\epsilon_{23}^2\right)^{1/2}/\epsilon_{22}. \tag{4}$$

In the above expressions k is the wavenumber in the z direction, $A(k)$ is the Fourier coefficient, and $j=\sqrt{-1}$. Equation (2) ensures the continuity of the potential at the vacuum–piezoelectric interface. The surface-charge density on the strips can be expressed as

$$\rho_s(z)=\frac{1}{2\pi}\int_{-\infty}^{+\infty}\rho(k)\exp\left(-jkz\right)dk \tag{5}$$

where

$$\rho(k)=\int_{-\infty}^{+\infty}\rho_s(z)\exp\left(jkz\right)dz \tag{6}$$

and the boundary condition at the interface is given by

$$D_y(0^+,z)-D_y(0^-,z)=\rho_s(z). \tag{7}$$

Using $\vec{D}=-\overleftrightarrow{\epsilon}\cdot\nabla V$ and (2) results in

$$A(k)=\rho(k)/\left[\epsilon_0(1+\alpha)|k|\right] \tag{8}$$

0018-9480/79/1100-0897$00.75 ©1979 IEEE

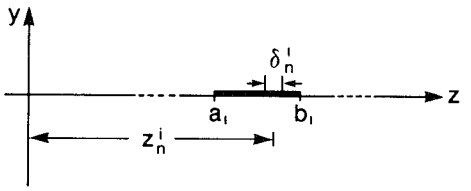

Fig. 2. The geometry relevant to the application of the moment method.

where

$$\alpha = \epsilon_{22}\epsilon_r/\epsilon_0. \tag{9}$$

II. Surface-Charge Density and Capacitance

For simplicity it is assumed that the transducer is geometrically symmetric and electrically asymmetric in respect to y axis, as shown in Fig. 1. This assumption produces an asymmetrical surface-charge density [2], [12]. Using (2) and (8) results in

$$\int_0^\infty \rho(k)\frac{\sin kz}{k}\,dk = j\pi\epsilon_0 V_l(1+\alpha)/2 \tag{10}$$

with $a_l \leqslant z \leqslant b_l$, $l=1,2,\cdots,M$, where a_l and b_l are the locations, and $V_l/2$ is the potential of the lth strip, as shown in Fig. 1, and where M is the number of electrode pairs. The ith strip, shown in Fig. 2, is divided into N_i subsections, and a function f_n^i is defined as

$$f_n^i = \begin{cases} 1, & \text{on } \delta_n^i \\ 0, & \text{elsewhere.} \end{cases} \tag{11}$$

The surface-charge density can be approximated by

$$\rho_s(z) = \rho_0 \sum_{i=1}^{M}\sum_{n=1}^{N_i} \alpha_n^i f_n^i \tag{12}$$

where ρ_0 is a normalizing constant. The Fourier transform of the surface-charge density, obtained by substitution of (12) into (6), is given by

$$\rho(k) = 4j\rho_0 \sum_{i=1}^{M}\sum_{n=1}^{N_i} \alpha_n^i \sin\left(k\delta_n^i/2\right)\sin\left(kz_n^i\right)/k \tag{13}$$

where

$$z_n^i = a_i - \delta_n^i/2 + \sum_{n=1}^{n}\delta_n^i \tag{14}$$

subject to condition

$$\sum_{n=1}^{N_i}\delta_n^i = b_i - a_i. \tag{15}$$

For a point-matching solution, (10) is satisfied at the middle of each subsection δ_n^i. Substituting (13) into (10) results in

$$\sum_{i=1}^{M}\sum_{n=1}^{N_i}\alpha_n^i L_{mn}^{il} = V_l \tag{16}$$

with $m=1,2,\cdots,N_l$, and $l=1,2,\cdots,M$, where

$$L_{mn}^{il} = 4\int_0^\infty \sin\left(k\delta_n^i/2\right)\sin\left(kz_n^i\right)\sin\left(kz_m^l\right)dk/(k^2L) \tag{17}$$

$$\rho_0 = \pi\epsilon_0(1+\alpha)/2L \tag{18}$$

and where L is the distance between the two electrodes in the middle of the transducer, as shown in Fig. 1. The integral (17) is easy to evaluate [13], and results in

$$\begin{aligned} L_{mn}^{il} = \Bigg\{ &\left(z_n^i + \frac{\delta_n^i}{2} + z_m^l\right)\ln\left(z_n^i + \frac{\delta_n^i}{2} + z_m^l\right) - \left(z_n^i - \frac{\delta_n^i}{2} + z_m^l\right) \\ &\cdot\ln\left(z_n^i - \frac{\delta_n^i}{2} + z_m^l\right) - \left(z_n^i + \frac{\delta_n^i}{2} - z_m^l\right)\ln\left|z_n^i + \frac{\delta_n^i}{2} - z_m^l\right| \\ &+ \left(z_n^i - \frac{\delta_n^i}{2} - z_m^l\right)\ln\left|z_n^i - \frac{\delta_n^i}{2} - z_m^l\right| \Bigg\} \Big/ L. \end{aligned} \tag{19}$$

Equation (16) represents a system of linear equations with α_n^i unknowns. The solution of the system and the use of (12) results in the value of the surface-charge density.

When the alternate electrodes are interconnected, the system (16) is solved for

$$V_l = (-1)^{l-1} \tag{20}$$

and the total capacitance of the transducer can be easily determined as

$$C = \rho_0 \sum_{i=1}^{M}\sum_{n=1}^{N_i}(-1)^{i-1}\alpha_n^i\delta_n^i. \tag{21}$$

Similarly, for the double-electrode configuration

$$V_l = \begin{cases} (-1)^{(l-1)/2}, & l \text{ odd} \\ (-1)^{(l-2)/2}, & l \text{ even} \end{cases} \tag{22}$$

in (16), and the total capacitance is given by

$$\begin{aligned} C = \rho_0 \Bigg\{ &\sum_{\substack{i=1 \\ (i \text{ odd})}}^{M}\sum_{n=1}^{N_i}(-1)^{(i-1)/2}\alpha_n^i\delta_n^i \\ &+ \sum_{\substack{i=2 \\ (i \text{ even})}}^{M}\sum_{n=1}^{N_i}(-1)^{(i/2)-1}\alpha_n^i\delta_n^i \Bigg\}. \end{aligned} \tag{23}$$

In calculating the capacitance, each strip is divided into 20 equal subsections. At a metallization ratio $a=0.5$, an increase of number of subsections from 20 to 40 increases the capacitance of a single pair of electrodes by 0.5 percent. Therefore, 20 subsections were adopted for each strip as a reasonable compromise between the accuracy and the speed of computation.

The normalized transducer capacitance per half-electrode pair, per unit width is defined as [2], [6]

$$C_n = 2C/(1+\alpha)M. \tag{24}$$

Equation (24) is plotted in Fig. 3 as a function of "a", for a single-electrode pair transducer (solid line) and, for an infinitely long [2] transducer (dotted line). It is seen that

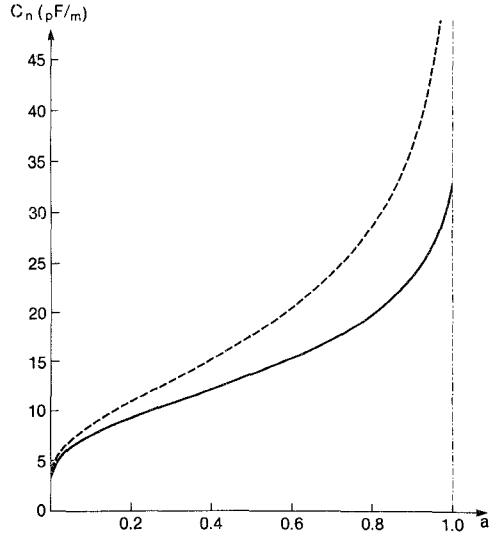

Fig. 3. The normalized transducer capacitance per half-electrode pair, per unit width, C_n as a function of the metallization ratio "a". Single-electrode pair transducer (solid line) and infinitely long transducer (dotted line).

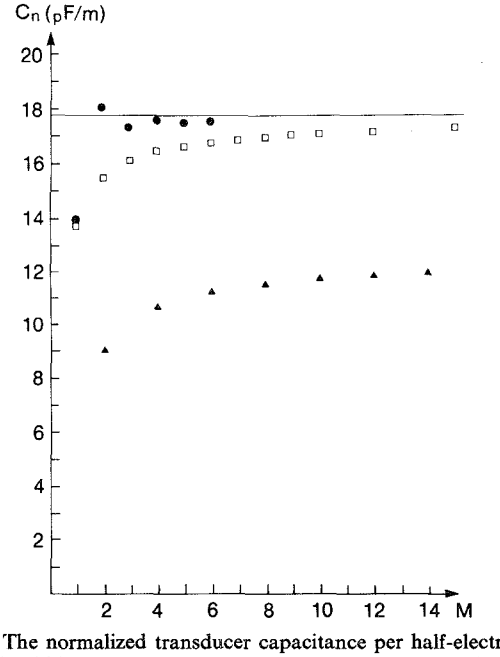

Fig. 4. The normalized transducer capacitance per half-electrode pair, per unit width, C_n as a function of number of electrode pairs M. C_n of the middle two electrodes in a $\lambda/4$ electrode transducer of M electrode pairs is shown by ●●●, and that of a $\lambda/4$ electrode transducer of M electrode pairs by □□□. Also shown with ▲▲▲ is the C_n of $\lambda/8$ electrode transducer of M electrode pairs.

the deviation between the two curves increases with the increase of "a". This suggests the importance of the end effects for short transducers especially at high-metallization ratios. Fig. 4 shows C_n of a uniform transducer for $\lambda/4$ electrode and $\lambda/8$ (double) electrode configurations, at $a=0.5$, as functions of the number of electrode pairs M. Also shown is the C_n of the two electrodes in the middle of a $\lambda/4$ electrode transducer. With increasing M, the C_n of the two middle electrodes approaches Engan's results for an infinite transducer very rapidly, while C_n of the overall transducer increases much slower. Thus it can be concluded that the total transducer capacitance depends on the end effects, even for a large number of fingers. Numerical results presented in Fig. 4 indicate that the increase in capacitance with the number of finger pairs, when the number of finger pairs exceeds three, is constant.

III. Field Distribution

The electric potential in the piezoelectric is obtained by substituting (8) and (13) into (2), and is given by

$$V(y,z)=\frac{1}{2}\sum_{i=1}^{M}\sum_{n=1}^{N_i}\alpha_n^i g_n^i(y,z) \tag{25}$$

where

$$g_n^i(y,z)=4\int_0^\infty \sin\left(k\delta_n^i/2\right)\sin\left(kz_n^i\right)\cdot\sin\left[k(z-\epsilon_{23}y/\epsilon_{22})\right]\exp\left(\epsilon_r ky\right)dk/(k^2L). \tag{26}$$

This results in a closed-form expression [13] for the potential at the interface given by

$$V(0,z)=\frac{1}{2L}\sum_{i=1}^{M}\sum_{n=1}^{N_i}\alpha_n^i\left\{\left(z_n^i+\frac{\delta_n^i}{2}+z\right)\ln\left(z_n^i+\frac{\delta_n^i}{2}+z\right)-\left(z_n^i-\frac{\delta_n^i}{2}+z\right)\ln\left(z_n^i-\frac{\delta_n^i}{2}+z\right)-\left(z_n^i+\frac{\delta_n^i}{2}-z\right)\cdot\ln\left|z_n^i+\frac{\delta_n^i}{2}-z\right|+\left(z_n^i-\frac{\delta_n^i}{2}-z\right)\ln\left|z_n^i-\frac{\delta_n^i}{2}-z\right|\right\} \tag{27}$$

which can be used for evaluation of the input admittance of interdigital transducer [14].

The components of the electric field in the piezoelectric are

$$E_y(y,z)=-\frac{1}{2}\sum_{i=1}^{M}\sum_{n=1}^{N_i}\alpha_n^i\frac{\partial}{\partial y}g_n^i(y,z) \tag{28}$$

and

$$E_z(y,z)=-\frac{1}{2}\sum_{i=1}^{M}\sum_{n=1}^{N_i}\alpha_n^i\frac{\partial}{\partial z}g_n^i(y,z) \tag{29}$$

where

$$\frac{\partial}{\partial y}g_n^i(y,z)=\left[\epsilon_r I_n^i(y,z)-\epsilon_{23}J_n^i(y,z)/\epsilon_{22}\right]/L \tag{30}$$

$$\frac{\partial}{\partial z}g_n^i(y,z)=J_n^i(y,z)/L \tag{31}$$

$$I_n^i(y,z)=4\int_0^\infty \sin\left(k\delta_n^i/2\right)\sin\left(kz_n^i\right)\cdot\sin\left[k(z-\epsilon_{23}y/\epsilon_{22})\right]\exp\left(\epsilon_r ky\right)dk/k \tag{32}$$

and

$$J_n^i(y,z)=4\int_0^\infty \sin\left(k\delta_n^i/2\right)\sin\left(kz_n^i\right)\cdot\cos\left[k(z-\epsilon_{23}y/\epsilon_{22})\right]\exp\left(\epsilon_r ky\right)dk/k. \quad (33)$$

Using standard integrations [13], (32) and (33) reduce to

$$I_n^i(y,z)=-\arctan\left[\frac{z_n^i+\frac{\delta_n^i}{2}+z-\frac{\epsilon_{23}y}{\epsilon_{22}}}{\epsilon_r|y|}\right]+\arctan\left[\frac{z_n^i+\frac{\delta_n^i}{2}-z+\frac{\epsilon_{23}y}{\epsilon_{22}}}{\epsilon_r|y|}\right]+\arctan\left[\frac{z_n^i-\frac{\delta_n^i}{2}+z-\frac{\epsilon_{23}y}{\epsilon_{22}}}{\epsilon_r|y|}\right]+\arctan\left[\frac{-z_n^i+\frac{\delta_n^i}{2}+z-\frac{\epsilon_{23}y}{\epsilon_{22}}}{\epsilon_r|y|}\right],\quad y<0 \quad (34)$$

and

$$J_n^i(y,z)=\frac{1}{2}\ln\left[\frac{(\epsilon_r y)^2+\left(z_n^i+\delta_n^i/2+z-\epsilon_{23}y/\epsilon_{22}\right)^2}{(\epsilon_r y)^2+\left(z_n^i-\delta_n^i/2+z-\epsilon_{23}y/\epsilon_{22}\right)^2}\right]+\frac{1}{2}\ln\left[\frac{(\epsilon_r y)^2+\left(z_n^i+\delta_n^i/2-z+\epsilon_{23}y/\epsilon_{22}\right)^2}{(\epsilon_r y)^2+\left(z_n^i-\delta_n^i/2-z+\epsilon_{23}y/\epsilon_{22}\right)^2}\right],\quad y<0. \quad (35)$$

Thus it is seen from (28) to (35) that the electric field is specified at any point in the piezoelectric, which is convenient for expressing the driving terms in the wave equation [1].

The potential and electric field of several electrode configurations, on Y–Z lithium niobate, were computed using the derived equations. For Y–Z lithium niobate, using (5), (13), (28), (30), and (32), it can be proven that the surface-charge density is proportional to the normal component of the electric field under the transducer, i.e.,

$$\rho_s(z)/\rho_0=-2E_y(0^-,z)L/\pi\epsilon_r. \quad (36)$$

Thus it is not necessary to plot $\rho_s(z)$ if $E_y(0^-,z)$ is known. Fig. 5(a) shows the potential and the electric field of the sequence $+-+-|+-+-$. Only half the sequence is shown since the potential and the normal component of the electric field are asymmetric while the tangential component of the electric field is symmetric. The same comment applies to the Fig. 5(b) and (c) as well. Fig. 5(b) shows a double electrode sequence $++--|++--$, and Fig. 5(c) a sequence $+-++-|+--+-$ with phase reversal.

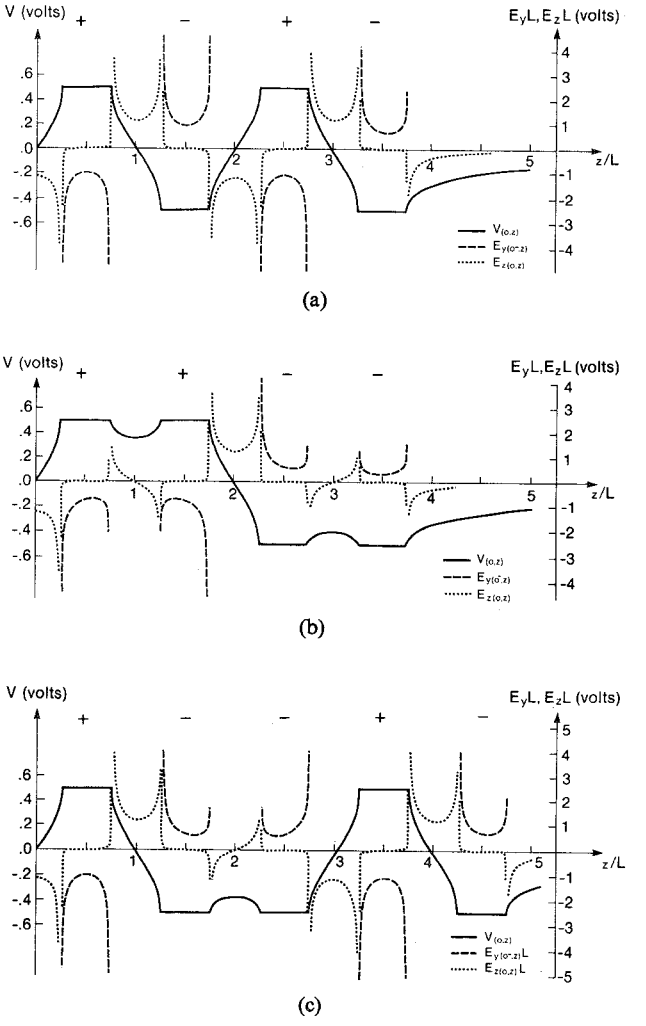

Fig. 5(a). The potential $V(0,z)$ the tangential electric field $E_z(0,z)$, and the normal electric field $E_y(0^-,z)$ as a function of normalized distance z/L for a sequence $+-+-|+-+-$. Only the RHS of the sequence is shown. (b) The potential $V(0,z)$, the tangential electric field $E_z(0,z)$, and the normal electric field $E_y(0^-,z)$ as a function of normalized distance z/L for a sequence $++--|++--$. Only the RHS of the sequence is shown. (c) The potential $V(0,z)$, the tangential electric field $E_z(0,z)$, and the normal electric field $E_y(0^-,z)$ as a function of normalized distance z/L for a sequence $+-++-|+--+-$. Only the RHS of the sequence is shown.

IV. Input Admittance

The moment-method technique can also be extended to determine the total input admittance of interdigital transducers taking the piezoelectric coupling into account [12]. The frequency dependence of the input admittance for Y–Z lithium niobate for different number of electrode pairs M is shown in Fig. 6(a) and (b) for resonant frequency of 100 MHz. As expected, the conductance, Fig. 6(a) increases at resonance with increasing number of electrode pairs. At resonance, the normalized conductance for a single pair of electrodes ($M=1$) is 23.6 ms/m, while for $M=2$ it becomes 33.4 ms/m, which is an increase of 42 percent. The conductance for $M=3$ is 51.2 ms/m, a 53-percent increase over that for $M=2$. For $M=4$, 5, and 6 the conductance is 66, 80.5, and 92.9 ms/m, respectively. The corresponding percentage increase is 29, 22, and 16 percent.

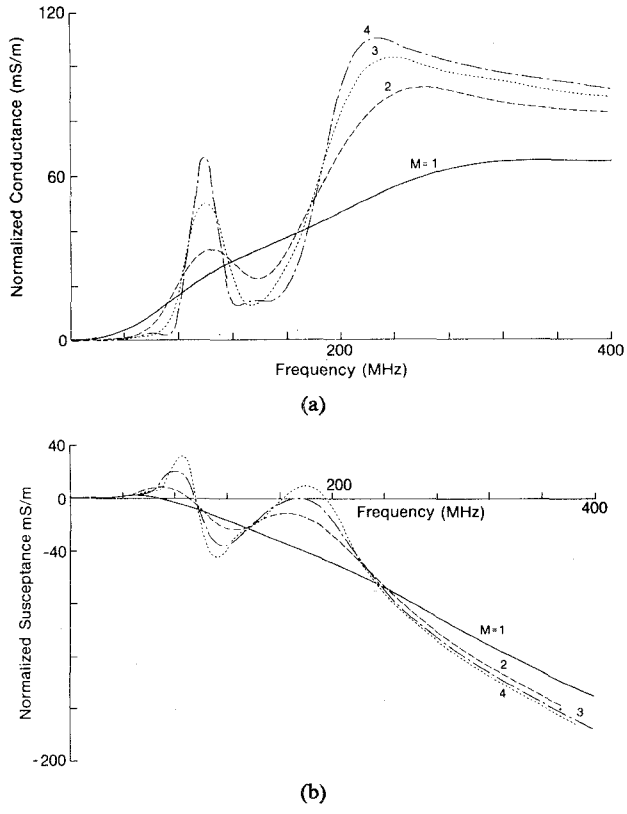

Fig. 6(a). The normalized input conductance versus frequency for different number of electrode pairs, M for Y–Z lithium niobate. The resonant frequency is 100 MHz, $L=17.44$ μm, and $a=0.5$. (b) The normalized input susceptance versus frequency for different number of electrode pairs, M for Y–Z lithium niobate. The resonant frequency is 100 MHz, $L=17.44$ μm, and $a=0.5$.

V. Conclusions

The finding of the surface-charge density and capacitance in finite transducers is greatly simplified with the moment-method technique. The contribution of the end effects to the total capacitance of the transducer is important in short transducer, especially for high-metallized ratios. The moment-method technique was also extended to include the piezoelectric coupling and to determine the input admittance of transducers with few finger pairs.

Closed-form expressions for the electric and potential fields was derived and then used to compute the potential, the tangential, and the normal components of the electric fields for three different transducer sequencies.

Numerical results presented indicate that the increase in capacitance with the number of finger pairs, when the number of finger pairs exceeds three, is constant.

References

[1] S. G. Joshi and R. M. White, "Excitation and detection of surface elastic waves in piezoelectric crystals," *J. Acoust. Soc. Amer.*, vol. 46, pt. 1, pp. 17–27, July 1969.

[2] H. Engan, "Excitation of elastic surface waves by spatial harmonics of interdigital transducers," *IEEE Trans. Electron Devices*, vol. ED-16, pp. 1014–1017, Dec. 1969.

[3] M. O. Vassell and A. K. Ganguly, "Electric field distribution for a surface interdigital transducer," *IEEE Trans. Electron Devices*, vol. ED-18, pp. 66–69, Jan. 1971.

[4] W. R. Smith and W. F. Pedler, "Fundamental and harmonic-frequency circuit-model analysis of interdigital transducers with arbitrary metalization ratios and polarity sequences," *IEEE Trans. Microwave Theory Tech.*, vol. MTT-23, pp. 853–864, Nov. 1975.

[5] H. Skeie and A. Ronnekleiv, "Electrostatic neighbour and end-effects in weighted surface wave transducers," in *Proc. 1976 IEEE Ultrasonics Symp.*, pp. 540–542.

[6] I. A. Cermak, P. Silvester, and S. K. Wong, "Capacitance determination for infinite interdigital structures," *IEEE Trans. Microwave Theory Tech.*, vol. MTT-18, p. 116, Feb. 1970.

[7] S. R. Ponamgi and H. Tuan, "Theoretical calculation of capacitance of an IDT over a piezoelectric layered structure," *IEEE Trans. Sonics Ultrason.*, vol. SU-21, pp. 125–127, Apr. 1974.

[8] A. Venema, J. J. M. Dekkers, and R. F. Humphryes, "Static capacitance calculations for a surface acoustic wave interdigital transducer in multilayered media," *IEEE Trans. Microwave Theory Tech.*, vol. MTT-26, pp. 294–297, Apr. 1978.

[9] C. S. Hartmann and B. G. Secrest, "End effects in interdigital surface wave transducers," in *Proc. 1972 IEEE Ultrasonics Symp.*, pp. 413–416.

[10] R. F. Harrington, *Field Computation by Moment Methods*. New York: Macmillan, 1968, ch. 2.

[11] R. S. Wagers, "Transverse electrostatic end effects in interdigital transducers," in *Proc. 1976 IEEE Ultrasonics Symp.*, pp. 536–539.

[12] A. M. Hussein and V. M. Ristic, "The evaluation of the input admittance of SAW interdigital transducers," *J. Appl. Phys.*, July 1979.

[13] I. S. Gradshteyn and I. M. Ryshik, *Table of Integrals, Series, and Products*. New York: Academic, 1965, pp. 422, 491–492.

[14] R. S. Wagers, "Evaluation of finger withdrawal transducer admittances by normal mode analysis," *IEEE Trans. Sonics Ultrason.*, vol. SU-25, pp. 85–92, Mar. 1978.